

Plasmonic nanoparticles assemblies templated by helical bacteria and resulting optical activity

Wenchun Feng^{1,2,3} | Usha Kadiyala^{2,4} | Jiao Yan^{2,3} | Yichun Wang^{2,5} |
Victor J. DiRita⁶ | J. Scott VanEpps^{2,4,5,7,8} | Nicholas A. Kotov^{2,3,5,7} 

¹US Food and Drug Administration, Silver Spring, Maryland, USA

²Biointerfaces Institute, University of Michigan, Ann Arbor, Michigan, USA

³Department of Chemical Engineering, University of Michigan, Ann Arbor, Michigan, USA

⁴Department of Emergency Medicine, University of Michigan, Ann Arbor, Michigan, USA

⁵Department of Biomedical Engineering, University of Michigan, Ann Arbor, Michigan, USA

⁶Department of Microbiology and Molecular Genetics, Michigan State University, East Lansing, Michigan, USA

⁷Michigan Center for Integrative Research in Critical Care, University of Michigan, Ann Arbor, Michigan, USA

⁸Macromolecular Science and Engineering Program, University of Michigan, Ann Arbor, Michigan, USA

Correspondence

Nicholas A. Kotov, Biointerfaces Institute,
Department of Chemical Engineering,
Department of Biomedical Engineering,
University of Michigan, Ann Arbor, MI
48109, USA.
Email: kotov@umich.edu

Funding information

National Science Foundation, Grant/
Award Number: 1463474; NIH, Grant/
Award Number: K08 AI128006; Air Force
Office of Scientific Research–funded
project, Grant/Award Number:
FA9550-16-1-0265; NSF-funded project,
Grant/Award Number: 1463474

Abstract

Plasmonic nanoparticles (NPs) adsorbing onto helical bacteria can lead to formation of NP helicoids with micron scale pitch. Associated chiroptical effects can be utilized as bioanalytical tool for bacterial detection and better understanding of the spectral behavior of helical self-assembled structures with different scales. Here, we report that enantiomerically pure helices with micron scale of chirality can be assembled on *Campylobacter jejuni*, a helical bacterium known for severe stomach infections. These organisms have right-handed helical shapes with a pitch of 1–2 microns and can serve as versatile templates for a variety of NPs. The bacteria itself shows no observable rotatory activity in the visible, red, and near-IR ranges of electromagnetic spectrum. The bacterial dispersion acquires chiroptical activity at 500–750 nm upon plasmonic functionalization with Au NPs. Finite-difference time-domain simulations confirmed the attribution of the chiroptical activity to the helical assembly of gold nanoparticles. The position of the circular dichroism peaks observed for these chiral structures overlaps with those obtained before for Au NPs and their constructs with molecular and nanoscale chirality. This work provides an experimental and computational pathway to utilize chiroplasmonic particles assembled on bacteria for bioanalytical purposes.

KEY WORDS

bacteria, biotechnology, *C. jejuni*, circular dichroism, gold nanoparticle, mesoscale, plasmonic, plasmonic, simulation

[This article is part of the Special Issue: In honor and memory of Prof. Koji Nakanishi. See the first articles for this special issue previously published in Volumes 31:12, 32:3, 32:4, 32:5, and 32:6. More special articles will be found in this issue as well as in those to come.]

1 | INTRODUCTION

Chirality is one of the most universal properties of the physical world.^{1–4} Chiral nanoscale structures from inorganic materials with strongly polarizable plasmonic and excitonic electronic states provide an avenue to efficiently manipulate polarization of light.^{5–14} Templated assemblies of plasmonic nanoparticles (NPs) using biomacromolecules can produce superstructures with nanoscale chiral geometries.^{14–20} However, the assemblies with micron-scale chiral geometries expected to be formed on live or dormant helical microorganisms would also be interesting. This research effort should extend scaling behavior for chiroptical properties of plasmonic structures to microscale. Furthermore, self-assembly of NPs^{21,22} into helices using biological templates may in perspective circumvent the problems of three-dimensional lithography,^{9,23,24} such as low throughput, due to efficient template assembly at the interfaces.²⁵ The assemblies of NPs on microscale organisms would also be interesting as a new experimental tool to observe the dynamics of the microorganisms. Last but not the least, the emergence of the chiroptical activity in the part of the spectrum where the biological structures typically have no noticeable circular dichroism peaks can also be utilized for rapid detection of bacterial infections.

Bacteria exhibit a wide range of sizes (usually on the micron scale) and shapes,²⁶ from spheres and rods of no apparent chirality to chiral asymmetric spirals such as those of *Campylobacter jejuni* (*C. jejuni*). In practical applications, the existence of chirality itself is not necessarily sufficient for its utilization in polarization-based devices. Many artificial systems are inherently racemic and chiroptically inactive, meaning that they exist as an equal amount of left- and right-handed species, which cancel out each other's optical activity. A chiroptical system must display enantiomeric excess (e.e.), where one species' handedness is dominant over the other in order to be chiroptically active in a specific region of electromagnetic spectrum.^{22,27,28} Asymmetric bacteria are nearly ideal experimental system in this case because they are enantiopure chiral microstructures. Both *C. jejuni*²⁹ and *Leptospira interrogans*³⁰ are known to have right-handed twist. Colonies of *Bacillus subtilis* are known to form right-handed microfibers at room temperature.³¹

There have been extensive studies using light to interrogate bacterial systems for their volumetric organism density by visible and near-infrared (NIR) light absorption, scattering, or diffraction.^{32–40} However, despite the prevalence of chirality in bacteria, the implication of their microscale chirality for optical properties is not yet well understood, and their enantiopure nature

is technologically underutilized.^{41–43} NP functionalization has been previously conducted on a variety of bacteria species,^{44–46} but until now, there have been no studies on plasmonic functionalization on chiral bacteria and associated chiroptical activity. In this work, we report plasmonic functionalization of *C. jejuni* and finite-difference time-domain (FDTD) simulations of their circular dichroism (CD) spectra. The results not only confirmed the expectation of the formation of microscale template helicoids, but also showed conformal Au NP shell enhance the chiroptical response. Overall, this study contributes to further understanding of chiroptical properties of helical bacteria; the findings can be used to advance chiral photonics and rapid detection of bacterial infections.

2 | MATERIALS AND METHODS

2.1 | Synthesis of Au NPs

Positively and negatively charged Au NPs in aqueous dispersions were synthesized according to previously published protocols with 2-aminoethanethiol and citrate as ligands, respectively.^{47,48} Their UV-Vis absorption spectra (Figure S1) were obtained using an Agilent/HP 8453 UV-Vis spectrophotometer, and their size and molar concentration were determined according to methods described by Khlebstov⁴⁹ and Liu⁵⁰ (positively charged Au NPs: 33 nm, 6.75×10^{-10} M; negatively charged Au NPs: 11 nm, 1.22×10^{-8} M).

2.2 | Synthesis of Au nanorods

The synthetic procedure was adapted with some modification from a method reported by Nikoobakht.⁵¹ Preparation of Au seed solution: Cetyltrimethylammonium bromide (CTAB)-capped seeds were prepared by chemical reduction of HAuCl₄ with NaBH₄: Freshly prepared, ice-cold NaBH₄ (0.01 M, 10 mL) was injected into a mixture of CTAB (0.1 M, 7.5 mL), HAuCl₄ (23 mM, 0.1 mL), and deionized water (1.8 mL) under magnetic stirring for 3 min. The color of the solution turned from yellow to brown, indicating the formation of Au seeds. The seed solution was kept undisturbed at 30°C for 2–5 h before use.

2.3 | Growth of Au nanorods

The Au nanorods (NRs) growth solution was made by mixing CTAB (0.1 M, 100 mL), HAuCl₄ (25 mM, 2 mL),

AgNO_3 (0.1 M, 120 μL), and ascorbic acid (AA, 0.1 M, 552 μL). The seed solution (120 μL) was added to the growth solution to initiate the growth of Au NRs. The well-mixed solution was kept undisturbed for 12 h, then AA (0.1 M, 552 μL) was added twice at 40-min intervals. The total reaction time was 24 h.

2.4 | Plasmonic functionalization

For positively charged Au NP functionalization, 1.25 mL *C. jejuni* (NCTC 11168, wild-type clinical strain) aqueous solution ($\text{OD} = 2.5$) was mixed with 5-mL Au NP solution and incubated for 10 min followed by a centrifuge step at 4000 rpm for 5 min. The precipitate was redispersed in 1.25 mL water and then used for CD spectroscopy. For negatively charged Au NP functionalization, the first step was to coat the bacteria with a layer of polydiallyldimethylammonium (PDDA), because the bacteria surface is negatively charged and the PDDA layer alters the surface charge to positive making it possible for the adsorption of negatively charged Au NPs. A total of 1.25 mL *C. jejuni* aqueous solution ($\text{OD} = 2.5$) was mixed with 5 mL PDDA (1 mg/mL, in 0.1 M NaCl) solution and incubated for 10 min, followed by a centrifuge step at 4000 rpm for 30 min. Then the precipitate was washed three times with 6.25 mL water at 4000 rpm for 15 min. Finally, the precipitate was redispersed in 1.25 mL water and mixed with 10 mL Au NP solution. This solution was allowed to incubate for 5 min before placing in a centrifuge at 4000 rpm for 5 min and then used for CD measurements.

2.5 | CD measurements

JASCO J-815 CD spectrophotometer was used for CD spectroscopy with the following scanning parameters: Scanning speed = 100 nm/min, data pitch = 0.1 nm, D.I.T. = 4 s, bandwidth = 1 nm, and number of accumulation = 1.

2.6 | Scanning electron microscopy imaging

After CD measurements, the bacteria solutions were subject to glutaraldehyde fixing and ethanol dehydration gradients. The final dehydrated sample solution was drop cast on a silicon wafer and imaged without sputter coating in scanning electron microscopy (SEM) (FEI Nova 200 Nanolab SEM/FIB).

2.7 | FDTD simulations

The CD, extinction, and g-factor spectra were calculated using a commercial FDTD software package (Lumerical Solutions Inc., <http://www.lumerical.com/tcad-products/fdtd/>). The structural model of the bacteria was constructed from Figure 1A in COMSOL with the following parameters: shape = helix, number of turns = 1, major radius = 112 nm, minor radius = 139 nm, axial pitch = 1300 nm, radial pitch = 0 nm, right-handed chirality, and end caps are perpendicular to spine. This model was then imported to 3ds Max, where Au NPs of 11 nm diameter were added onto the surface of the bacteria with a spacing of 28 nm between the center of each NP corresponding to the distances between the NPs observed in the samples by electron microscopy. The mesh type is auto nonuniform with a mesh size of 1.5 nm along all the three axes and a mesh accuracy of 3. The circularly polarized light irradiation is along the axial direction of the helical model structure. Simulation environment was in water ($n_{\text{water}} = 1.33$). The refractive index of *C. jejuni* was estimated from that of *Escherichia coli* ($n=1.388$).⁵² Refractive index of Au is derived from Johnson and Christy (LUMERICAL database).⁵³

3 | RESULTS AND DISCUSSION

3.1 | Self-assembly of nanoscale colloids on bacterial surface

C. jejuni is a helical bacterium with a curvy rod shape (Figure 1A) and is one of the most common causes of gastroenteritis around the globe.^{54,55} At the onset of the study, we hypothesized that this bacteria can be used as a template for the self-assembly of the plasmonic NPs or other nanoscale colloids, such as nanorods (NRs), into helices that should lead to chiroptical activity in the red part of the spectrum. The challenge for this project was successful deposition of the NPs or NRs on to the bacterium while retaining its curvy rod shape. Note that helical shape is typical only for live *C. jejuni*, and they convert to mostly achiral rod-like shape under stress.

Self-assembly on bacterial surface was carried out for of positively and negatively charged Au nanocolloids. Because the surface of bacteria is typically negatively charged, we started with the direct adsorption of positively charged NPs. However, we observed nonuniform deposition of the NPs attributed to the uneven charge distribution on the bacterial surfaces (Figure 1B).⁴⁵

Deposition of the negatively charged NPs followed a layer-by-layer (LBL) assembly that was previously successful in coating bacteria.^{44–46,56,57} After one layer of

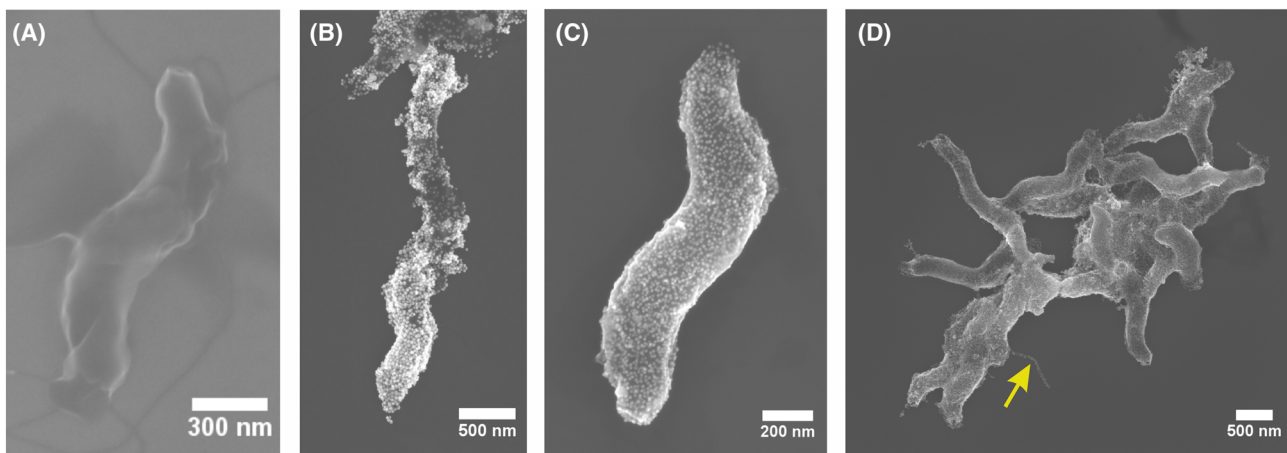


FIGURE 1 SEM images of (A) *C. jejuni*, (B) coated with positively charged Au NPs, and (C-D) coated with negatively charged Au NPs (yellow arrow points to a coated flagellum). SEM, scanning electron microscopy

polydiallyldimethylammonium (PDDA) deposition on the bacteria, the negatively charged Au NPs can then be completely deposited on top of PDDA. The PDDA layer imparted a uniform positive charge (zeta potential shown in Figure S2) throughout the surface of the bacteria, and the subsequent negatively charged Au NPs adsorbed onto this layer with much higher uniformity compared with those of the positively charged Au NPs (Figure 1C,D). The uniformity of the coating is particularly significant in light of subsequent modeling of the chiroptical properties of these particulate helicoids.

3.2 | Optical properties

Looking into the optical properties of the bacterium-templated NP assemblies, except for *E. coli*, the refractive index for most other bacteria species is unknown; therefore, we approximated the refractive index of *C. jejuni* with that of *E. coli* ($n=1.388$). Considering that bacteria mostly consist of water which should lead to a refractive index close to that of water at 1.33, the approximation most likely holds true. Although *C. jejuni* is a helical bacterium, because its refractive index is close to that of water, there is no rotatory power in the visible region for bacterial dispersion (Figure 2A). There is chiroptical activity in the UV region (200–400 nm) due to the proteins and other biomolecular components in the bacterium; however, this chiroptical activity is not specific to the bacteria, making the analysis of the corresponding CD spectra from various bacterial species less informative than for, say individual amino acids, drug enantiomers, or chiral NPs.

After plasmonic functionalization with either positively or negatively charged Au NPs, the bacteria acquired detectable rotatory power in the visible region

of electromagnetic spectrum between 500 and 750 nm, which, of course, was not observed before in any bacterial species. The chiroptical response for both types of Au NPs is positive and the chiral anisotropy (g) factor is around 1×10^{-4} and 2×10^{-4} for positively and negatively charged Au NPs, respectively.

The question now is what scale of chirality these CD peaks can be attributed to. They may originate from the local enhancement of CD activity of the chiral biomolecules due to the weak but noticeable hybridization of excitonic and plasmonic states on biomolecules and NPs.⁵⁸ To answer this question, symmetrically shaped bacteria, namely, *E. coli* and *Staphylococcus aureus*, were coated with positively charged Au NPs following the same procedure, but none of the products showed any observable chiroptical activity from 500 to 750 nm within the sensitivity of the state-of-the-art instrumentation for chiroptical measurements (Figure S3). This indicated that this CD peak does not correspond to the chiroplasmonic activity of local complexes of NP with proteins or other biomolecules. This experiment also showed the necessity of the curvy rod shape of *C. jejuni* for the induction of rotatory power at the 500–750 nm CD band.

The chiroptical activity between the coatings made from positively and negatively charged NPs is similar, though the positively charged Au NPs coated bacteria showed a slightly higher scattering background in the absorption spectrum compared to the negatively charged ones (Figure 2B). Again, this fact is likely to be attributed to some degree of aggregation of the bacteria because the NP layer can increase supramolecular and electrostatic attraction between two or more organisms. One also needs to consider that positively charged NPs adsorb directly on to the surface of bacteria which is likely to have uneven charge distribution, whereas the negative Au NPs attach onto the relative uniform charged surface

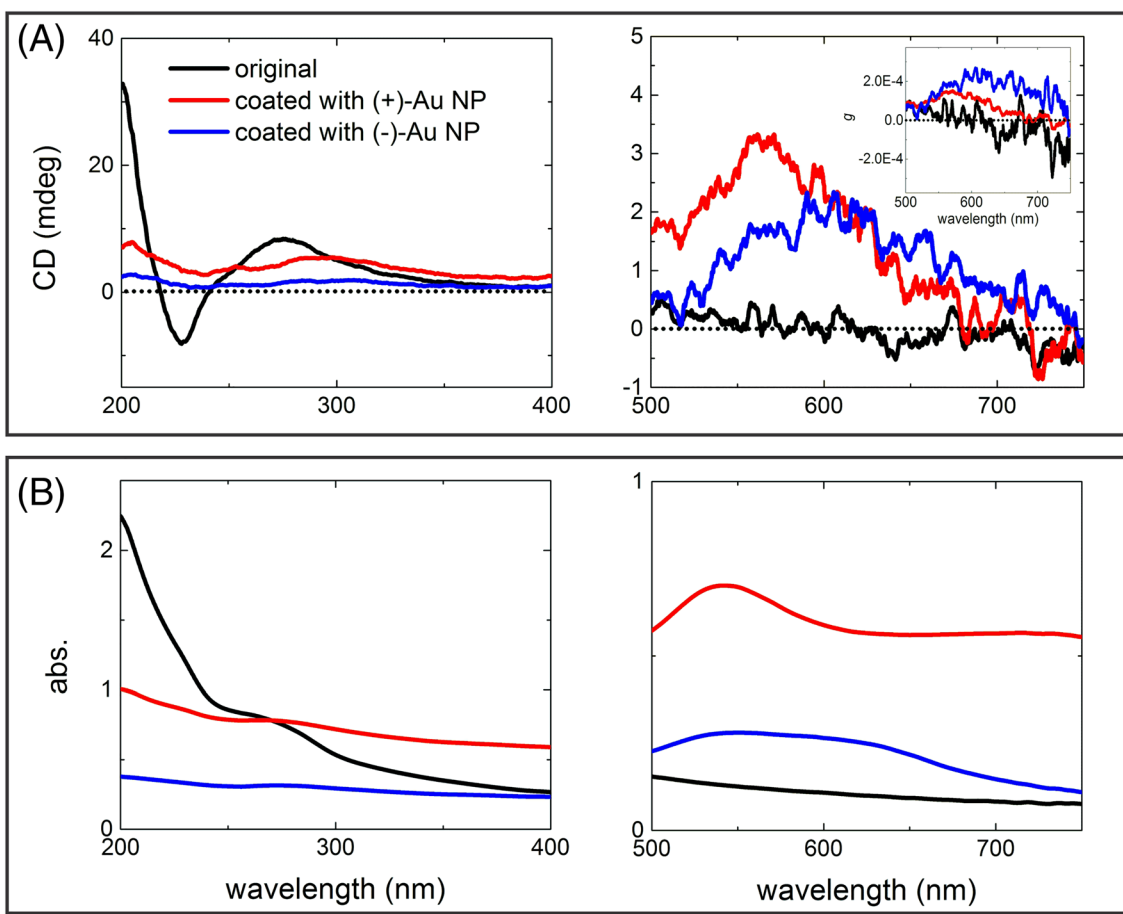


FIGURE 2 (A) CD and (B) absorbance spectra in UV (left graphs) and visible (right graphs) parts of the spectrum for *C. jejuni* before and after being coated with positively or negatively charged Au NPs. Inset in the CD spectrum for the visible spectral part shows the corresponding g-factor spectra

primed by PDDA. Notably, the overall chiroptical activity is relatively weak, which is associated with the mismatch between the characteristic pitch of *C. jejuni* in the micron range and the submicron wavelengths of photons in the visible part of the spectrum available for measurements at the moment. Although the weakness of the visible response is somewhat discouraging, the data presented in Figures 1 and 2 provide proof-of-concept for the formation of chiroptically active superstructures using the convenient shape of bacteria. The prior studies on chiral nano- and mesoscale structures indicate that once the origin of the CD peaks is uncovered, it can be further enhanced by numerous means for analytical and other purposes.

To confirm generality of the observed chiroptical response and its spectral tunability, *C. jejuni* was also coated with Au NRs. These test samples also exhibited moderate chiroptical response (~4 mdeg) at wavelengths further in the red part of the electromagnetic spectrum, namely, between 600 and 700 nm, corresponding to plasmonic resonance for Au NRs (Figure S4a,b). This indicates broad applicability in terms of the

functionalizing nanomaterials that can be used on the surface of *C. jejuni*. Furthermore, Au NR coatings on chiral templates are known to enhance CD amplitudes compared with Au NPs due to stronger plasmon-plasmon interactions.⁵⁹ Further methods of enhancement of the chiroptical activity can be related to better preservation of the curvy shape of the bacteria that may be damaged (Figure S4c) by the CTAB surfactant on the Au NRs.⁶⁰

3.3 | Simulations

Simulations can also confirm the origin of the chiroptical activity and determine the methods for further augmentation of the bacteria's CD spectra. A conformal layer of NPs similar to the one observed in Figure 1C lead to distinct CD peak in the plasmonic part of the spectrum (Figure 3) whose position matches that observed experimentally. Simulations also revealed that a complete layer of Au coating around *C. jejuni* can afford the IR part of the spectrum with great amplitude of polarization rotation (Figure S5). Bacteria coated with the NP shell

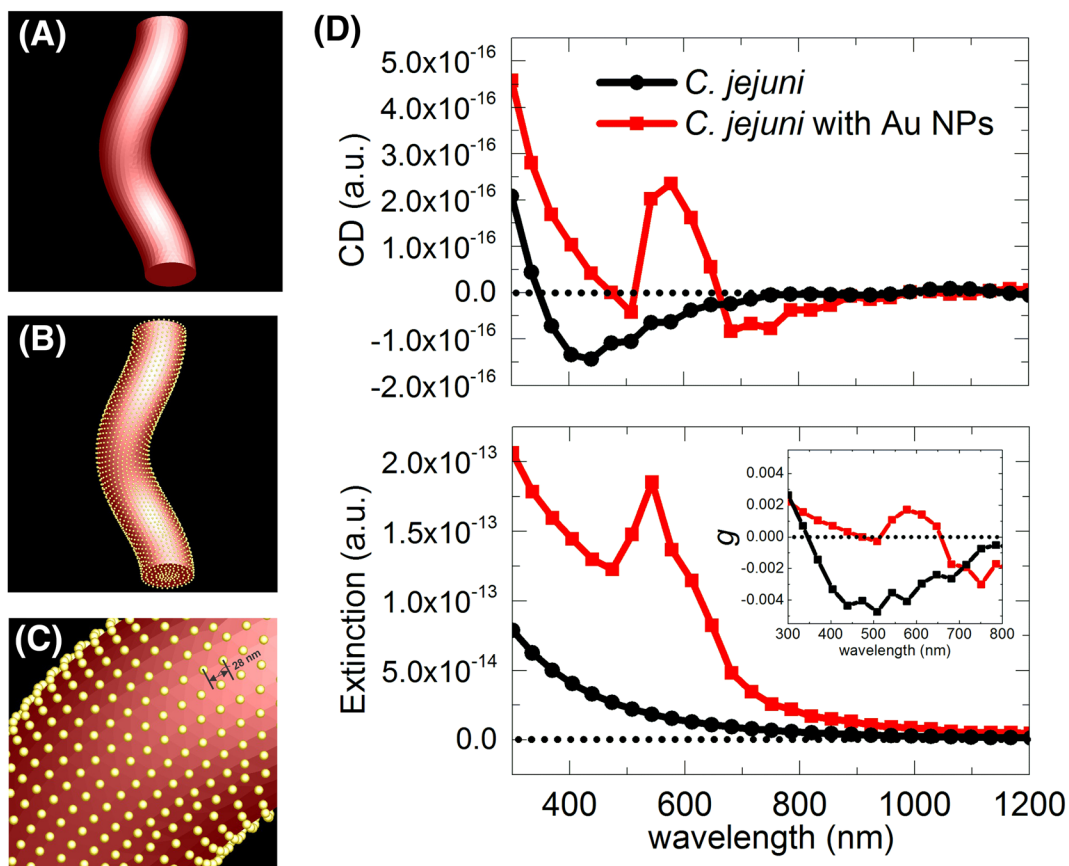


FIGURE 3 Simulation model of (A) *C. jejuni* and (B) *C. jejuni* coated with Au NPs with a magnified view in (C). (D) Simulated CD and extinction spectra of *C. jejuni* with and without Au NPs coating. Inset shows the calculated g-factor spectra

exhibited significantly higher chiroptical response due to the overall shape compared with other sources of chiroptical activity⁵ due to stronger field coupling between the Au NPs.

4 | CONCLUSION

Helical bacteria, either as individual cells, can be used as to guide self-assembly of plasmonic nanocomponents toward the formation of enantiopure helicoids, thus circumventing the problem of subtlety of chiral interactions known from chiral chemistry. We found that the chiroptical activity of the Au NP assemblies with mesoscale chiral geometries templated by *C. jejuni* are similar to those with nanoscale and molecular scale chirality, which is related to the dominance of the plasmonic absorption for CD bands in the visible and near infrared parts of the spectrum. Although functionalization of helical bacteria with nanoscale colloids, such as NPs and NRs, may provide a biotechnological pathway for the templating mesoscale chiroplasmonic

structures, it is not likely to compete with lithography. However, it may be suitable for bacterial detection which acquires increasing significance both with the microbiome studies and the rise of antibiotic resistance. Furthermore, these studies also open the door to new applications of chiroplasmonic effects for monitoring of shape changes of bacteria^{61–63} and time-resolved studies of NP interactions with bacteria.^{64,65} Extension of the spectral window of chiroptical spectroscopy to far-IR or terahertz⁶⁶ spectral range will further increase the sensitivity due to the stronger polarization rotation for longer wavelengths.

ACKNOWLEDGMENTS

The authors would like to thank the University of Michigan's Michigan Center for Materials Characterization for its assistance with scanning electron microscopy. The central part of this work was supported by the National Science Foundation funded project “Energy- and cost-efficient manufacturing employing nano-particles” (grant no. 1463474). Additional support acknowledged to NIH K08 AI128006.

ORCID

Nicholas A. Kotov  <https://orcid.org/0000-0002-6864-5804>

REFERENCES

1. Nakanishi K, Berova N, Woody RW. *Circular Dichroism: Principles and Applications*. Wiley-VCH; 2000.
2. Miles AJ, Whitmore L, Wallace BA. Spectral magnitude effects on the analyses of secondary structure from circular dichroism spectroscopic data. *Protein Sci.* 2005;14(2):368-374.
3. Yeom J, Santos U, Chekini M, Cha M, de Moura AF, Kotov NA. Chirodynamic nanoparticles and gels. *Science*. 2018;359(6373):309-314.
4. Morrow SM, Bissette AJ, Fletcher SP. Transmission of chirality through space and across length scales. *Nat Nanotechnol*. 2017; 12:410-419.
5. Ma W, Xu L, de Moura AF, et al. Chiral inorganic nanostructures. *Chem Rev.* 2017;117(12):8041-8093.
6. Guerrero-Martínez A, Alonso-Gómez JL, Auguié B, Cid MM, Liz-Marzán LM. From individual to collective chirality in metal nanoparticles. *Nano Today*. 2011;6:381-400.
7. Xia Y, Zhou Y, Tang Z. Chiral inorganic nanoparticles: Origin, optical properties and bioapplications. *Nanoscale*. 2011; 3:1374-1382.
8. Oaki Y, Imai H. Amplification of chirality from molecules into morphology of crystals through molecular recognition. *J Am Chem Soc.* 2004;126(30):9271-9275.
9. Mark AG, Gibbs JG, Lee T-C, Fischer P. Hybrid nanocolloids with programmed three-dimensional shape and material composition. *Nat Mater.* 2013;12(9):802-807.
10. Zhou Y et al. Biomimetic Hierarchical Assembly of Helical Supraparticles from Chiral Nanoparticles. *ACS Nano*. 2016;10 (3):3248-3256.
11. Singh G, Chan H, Baskin A, et al. Self-assembly of magnetite nanocubes into helical superstructures. *Science*. 2014;345 (6201):1149-1153.
12. Duan Y, Han L, Zhang J, et al. Angewandte optically active nanostructured ZnO films. *Angew*. 2015;54(50):15170-15175.
13. Kim Y, Yeom B, Arteaga O, et al. Reconfigurable chiroptical nanocomposites with chirality transfer from the macro- to the nanoscale. *Nat Mater.* 2016;15(4):461-468.
14. Yan J, Feng W, Kim J-Y, et al. Self-assembly of chiral nanoparticles into semiconductor helices with tunable near-infrared optical activity. *Chem Mater.* 2020;32(1):476-488.
15. Lan X, Lu X, Shen C, Ke Y, Ni W, Wang Q. Au nanorod helical superstructures with designed chirality. *J Am Chem Soc.* 2015; 137(1):457-462.
16. Chen W, Bian A, Agarwal A, et al. Nanoparticle superstructures made by polymerase chain reaction: Collective interactions of nanoparticles and a new principle for chiral materials. *Nano Lett.* 2009;9(5):2153-2159.
17. Mastroianni AJ. Pyramidal and chiral grouping of gold nanocrystals assembled using DNA scaffolds. *J Am Chem Soc.* 2010; 131;(24):8455-8459.
18. Hou K, Ali W, Lv J, et al. Optically active inverse opal photonic crystals. *J Am Chem Soc.* 2018;140(48):16446-16449.
19. Lv J, Ding D, Yang X, et al. Biomimetic chiral photonic crystals. *Angew Chem Int Ed*. 2019;58(23):7783-7787.
20. Lv J, Hou K, Ding D, et al. Gold nanowire chiral ultrathin films with ultrastrong and broadband optical activity. *Angew Chem Int Ed*. 2017;56(18):5055-5060.
21. Yeom J, Yeom B, Chan H, et al. Chiral templating of self-assembling nanostructures by circularly polarized light. *Nat Mater.* 2015;14(1):66-72.
22. Feng W, Kim JY, Wang X, et al. Assembly of mesoscale helices with near-unity enantiomeric excess and light-matter interactions for chiral semiconductors. *Sci Adv.* 2017;3(3): e1601159.
23. Gansel JK, Thiel M, Rill MS, et al. Gold helix photonic metamaterial as broadband circular polarizer. *Science*. 2009;325 (5947):1513-1515.
24. Esposito M, Tasco V, Todisco F, et al. Triple-helical nanowires by tomographic rotatory growth for chiral photonics. *Nat Commun.* 2015;6(1):6484.
25. Kotov NA. Self-assembly of inorganic nanoparticles: ab ovo. *Europhys Lett*. 2017;119:66008.
26. Hug LA, Baker BJ, Anantharaman K, et al. A new view of the tree and life's diversity. *Nat Microbiol*. 2016;1(5):16048.
27. Zhang J, Feng W, Zhang H, et al. Multiscale deformations lead to high toughness and circularly polarized emission in helical nacre-like fibres. *Nat Commun*. 2016;7(1):10701.
28. Roche C, Sun HJ, Prendergast ME, et al. Homochiral columns constructed by chiral self-sorting during supramolecular helical organization of hat-shaped molecules. *J Am Chem Soc.* 2014; 136:7169-7185.
29. Fields, P. & Fitzgerald, C. *Campylobacter jejuni*. (2004). <https://phil.cdc.gov/Details.aspx?pid=5778>
30. Carleton O, Charon NW, Allender P, O'Brien S. Helix handedness of Leptospira interrogans as determined by scanning electron microscopy. *J Bacteriol*. 1979;137(3):1413-1416.
31. Mendelson NH, Karamata D. Inversion of helix orientation in *Bacillus subtilis* macrofibers. *J Bacteriol*. 1982;151(1):450-454.
32. Ferrari GM, Tassan S. A method for the experimental determination of light absorption by aquatic heterotrophic bacteria. *J Plankton Res*. 1998;20:757-766.
33. Katz A, Alimova A, Min Xu, et al. Bacteria size determination by elastic light scattering. *IEEE J Sel Top Quantum Electron*. 2003;9(2):277-287.
34. Xu, M. & Katz, A. Statistical interpretation of light anomalous diffraction by small particles and its applications in bio-agent detection and monitoring. in *Light Scattering Reviews 3* 27-67 (Springer, 2008).
35. Balch WM, Vaughn JMJ, Novotny JF, et al. Fundamental changes in light scattering associated with infection of marine bacteria by bacteriophage. *Limnol Oceanogr*. 2002;47(5):1554-1561.
36. Sánchez O, Mas J. Light absorption by phototrophic bacteria: effects of scattering, cell concentration and size of the culture vessel. *Int Microbiol*. 1999;2(4):233-240.
37. Waltham C, Boyle J, Ramey B, Smit J. Light scattering and absorption caused by bacterial activity in water. *Appl Optics*. 1994;33(31):7536-7540.
38. Ulloa O, Sathyendranath S, Platt T, Quiñones RA. Light scattering by marine heterotrophic bacteria. *J Geophys Res*. 1992; 97:9619-9629.
39. Krepelka, P., Martos, F. C., Posada-Izquierdo, G. D. & Pérez-Rodríguez, F. Measuring and application of NIR light

- absorption coefficient of bacteria. in *Progress in Electromagnetics Research Symposium* 2336–2339 (2014).
40. Bateman JB, Wagman J, Carstensen EL. Refraction and absorption of light in bacterial suspensions. *Kolloid-Zeitschrift Und Zeitschrift für Polym.* 1966;208:44–58.
 41. Wang S, Furchtgott L, Huang KC, Shaevitz JW. Helical insertion of peptidoglycan produces chiral ordering of the bacterial cell wall. *Proc Natl Acad Sci U S A.* 2012;109(10): E595–E604.
 42. Ben-Jacob E, Cohen II, Shochet O, Tenenbaum A, Czirók A, Vicsek T. Cooperative formation of chiral patterns during growth of bacterial colonies. *Phys Rev Lett.* 1995;75(15):2899–2902.
 43. Mijalkov M, Volpe G. Sorting of chiral microswimmers. *Soft Matter.* 2013;9:6376–6381.
 44. Fakhrullin RF, Zamaleeva AI, Minullina RT. Cyborg cells: Functionalisation of living cells with polymers and nanomaterials. *Chem Soc Rev.* 2012;41(11):4189–4206.
 45. Fakhrullin RF, Lvov YM. “Face-lifting” and “make-up” for microorganisms: Layer-by-layer polyelectrolyte Nanocoating. *ACS Nano.* 2012;6(6):4557–4564.
 46. Kahraman M, Zamaleeva AI. Layer-by-layer coating of bacteria with noble metal nanoparticles for surface-enhanced Raman scattering. *Anal Bioanal Chem.* 2009;395(8):2559–2567.
 47. Niidome T, Nakashima K, Takahashi H, Niidome Y. Preparation of primary amine-modified gold nanoparticles and their transfection ability into cultivated cells. *Chem Commun (Camb).* 2004;1978–1979. <https://doi.org/10.1039/b406189f>
 48. Kim Y, Zhu J, Yeom B, et al. Stretchable nanoparticle conductors with self-organized conductive pathways. *Nature.* 2013;500 (7460):59–63.
 49. Khlebtsov NG. Determination of size and concentration of gold nanoparticles from extinction spectra. *Anal Chem.* 2008;80(17): 6620–6625.
 50. Liu X, Atwater M, Wang J, Huo Q. Extinction coefficient of gold nanoparticles with different sizes and different capping ligands. *Colloids Surf B Biointerfaces.* 2007;58(1):3–7.
 51. Nikoobakht B, El-sayed MA. Preparation and growth mechanism of gold nanorods (NRs) using seed-mediated growth method. *Chem Mater.* 2003;15:1957–1962.
 52. Liu PY, Chin LK, Ser W, et al. Real-time measurement of single bacterium's refractive index using optofluidic immersion refractometry. *Procedia Eng.* 2014;87:356–359.
 53. Johnson PB, Christy RW. Optical constants of the noble metals. *Phys Rev B.* 1972;6:4370–4379.
 54. Epps SV, Harvey RB, Hume ME, Phillips TD, Anderson RC, Nisbet DJ. Foodborne campylobacter: Infections, metabolism, pathogenesis and reservoirs. *Int J Environ Res Public Health.* 2013;10(12):6292–6304.
 55. Altekruze SF, Stern NJ, Fields PI, Swerdlow DL. Campylobacter jejuni—an emerging foodborne pathogen. *Emerg Infect Dis.* 1999;5(1):28–35.
 56. Park JH, Hong D, Lee J, Choi IS. Cell-in-shell hybrids: Chemical nanoencapsulation of individual cells. *Acc Chem Res.* 2016; 49(5):792–800.
 57. Seisenbaeva GA, Moloney MP, Tekoriute R, et al. Biomimetic synthesis of hierarchically porous nanostructured metal oxide microparticles—potential scaffolds for drug delivery and catalysis. *Langmuir.* 2010;26(12):9809–9817.
 58. Lee J, Govorov AO, Dulka J, Kotov NA. Bioconjugates of CdTe nanowires and Au nanoparticles: Plasmon-exciton interactions, luminescence enhancement and collective effects. *Nano Lett.* 2004;4(12):2323–2330.
 59. Guerrero-Martínez A, Auguié B, Alonso-Gómez JL, et al. Intense optical activity from three-dimensional chiral ordering of plasmonic nanoantennas. *Angew Chem Int Ed Engl.* 2011;50 (24):5499–5503.
 60. Tarantola M, Pietuch A, Schneider D, et al. Toxicity of gold-nanoparticles: Synergistic effects of shape and surface functionalization on micromotility of epithelial cells. *Nanotoxicology.* 2011;5(2):254–268.
 61. French S, Cote J-P, Stokes JM, Truant R, Brown ED. Bacteria getting into shape: Genetic determinants of *E. coli* morphology. *MBio.* 2017;8:e01977–16.
 62. Young KD. Bacterial morphology: Why have different shapes? *Curr Opin Microbiol.* 2007;10(6):596–600.
 63. Cabeen MT, Jacobs-Wagner C. Bacterial cell shape. *Nat Rev Microbiol.* 2005;3(8):601–610.
 64. Hajipour MJ, Fromm KM, Ashkarran AA, et al. Antibacterial properties of nanoparticles. *Trends Biotechnol.* 2012;30(10): 499–511.
 65. Cha S-H, Hong J, McGuffie M, Yeom B, VanEpps J, Kotov NA. Shape-dependent biomimetic inhibition of enzyme by nanoparticles and their antibacterial activity. *ACS Nano.* 2015; 9(9):9097–9105.
 66. Choi WJ, Cheng G, Huang Z, Zhang S, Norris TB, Kotov NA. Terahertz circular dichroism spectroscopy of biomaterials enabled by kirigami polarization modulators. *Nat Mater.* 2019; 18:826–829.

SUPPORTING INFORMATION

Additional supporting information may be found online in the Supporting Information section at the end of this article.

How to cite this article: Feng W, Kadiyala U, Yan J, et al. Plasmonic nanoparticles assemblies templated by helical bacteria and resulting optical activity. *Chirality.* 2020;32:899–906. <https://doi.org/10.1002/chir.23225>